Wind field structure and speed from Radarsat SAR images

P.W. Vachon[1], I. Chunchuzov[1]* & F.W. Dobson[2]

[1]Natural Resources Canada, Canada Centre for Remote Sensing
588 Booth Str., Ottawa, K1A 0Y7 Canada

[2] Canada Dept. of Fisheries & Oceans, Bedford Institute of Oceanography
P.O.Box 1006, Dartmouth, N.S. B2Y 4A2 Canada

* Under contract to CCRS from Noetix Research Inc.. 265 Carling Ave., Suite 403. Ottawa, Ont. K1S 2E1 Canada.

Two examples of Radarsat ScanSAR wide images of mesoscale cyclones in the Labrador Sea are presented, along with wind retrieval validation results from both the ERS SARs and the Radarsat SAR. The results show that SAR images may be used to deduce information about both the spatial structure and the wind speed of mesoscale phenomena near the ocean's surface.

Introduction

It has been well established that Synthetic Aperture Radar (SAR) images over the ocean can provide wind information over small spatial scales. SAR image data can be used quantitatively as an imaging scatterometer if the SAR is calibrated and a suitable wind retrieval model is available [*Vachon & Dobson* 1996; *Wackerman et al.* 1996; *Fetterer et al.* 1998]. Canada's Radarsat SAR (C-band HH polarisation) with its ScanSAR wide mode characterised by a swath width of 500 km at a spatial resolution of 100 m, can provide both synoptic-scale and small-scale views of the imprint of mesoscale meteorological processes and features on the ocean's surface.

Atmospheric mesoscale cyclonic vortices that develop in the regions between sea ice (or cold land) and the ocean during cold air outbreaks are of increasing interest [*Twitchell et al.* 1989; *Heinemann & Claud* 1997; *Mitnik et al.* 1996]. Often referred to as polar lows, intensive mesoscale cyclones are formed poleward of major jet streams in cold air masses or frontal zones; their cloud mass is mainly convective in origin [*Businger & Reed* 1989]. With small spatial scales (< 500 km) and short life times (24 to 48 hours), it may be difficult for numerical weather prediction models to fully simulate their initiation, temporal evolution, and spatial structure. Since polar mesoscale cyclones usually occur in data sparse regions, satellite images have been an important tool for the detection and characterisation of these phenomena [*Heinemann & Claud* 1997; *Mitnik et al.* 1996]. These high-latitude outbreaks also have a role in understanding and quantifying the intense fluxes of heat and moisture from sea to air that accompany oceanic deep convection [*Marshall et al.* 1998].

In this paper, we consider two such features observed in (thus far) uncalibrated Radarsat ScanSAR images. We then consider the more generic issue of wind retrieval from Radarsat SAR images and present wind speed validation results from single-beam mode observations taken over ships and buoys.

Labrador Sea mesoscale cyclones

Figure 1 shows a Radarsat ScanSAR wide image of an intense mesoscale cyclone (MC) over the Labrador Sea. The image was acquired for routine ice surveillance [*Bradley et al.* l998] on 29 December 1997. On this date, the sea-

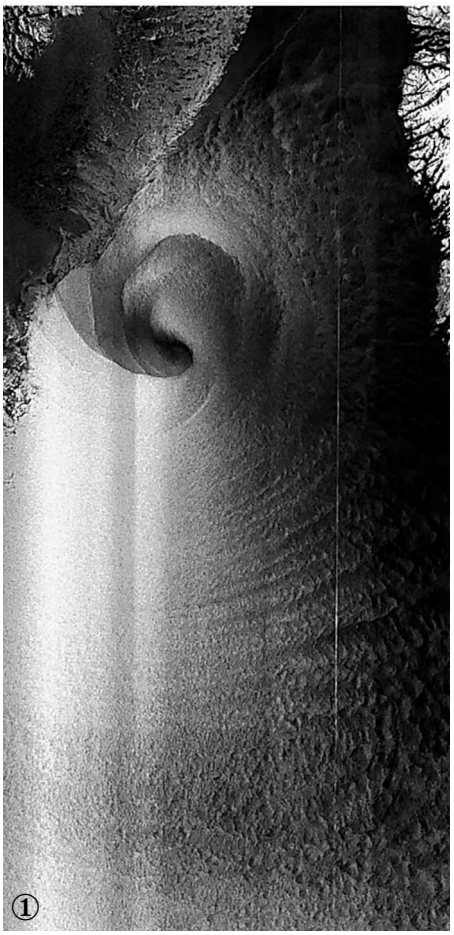

Ascending pass Radarsat ScanSAR wide image of northern Labrador Sea between Baffin Island and Greenland acquired 29 Dec.1997 at 21:19 UTC. The image covers 500 · 1000 km and was supplied courtesy of Canadian Ice Services. (SAR data ©CSA 1997)

level pressure charts indicate the existence of a cyclone between Baffin Island and Greenland. The Radarsat image shows, in detail, the spiral-form structure of the surface wind field around the 'eye' (the dark ellipsoid-shaped pattern) of the polar MC. The surface wind convergence zone at the core of the MC is characterised by sharp wind field gradients across the frontal boundary that converges towards the 'eye'. According to coastal weather stations, a strong, very cold western wind was blowing across the ice edge throughout 29 December. The advection of cold air from Baffin Island to the warmer open water is apparent as the bright area in the image. The strong airflow becomes organised downstream from the ice edge into a second-order flow with roll vortices that are seen on the image as spiral-form cloud streets. The spatial evolution of the cloud streets is characterised by an increase in the aspect ratio of the roll vortices downstream from the ice edge, due mainly to deepening of the boundary layer [*Hartmann et al.* 1997]. Deep cellular convection is evident north of the 'eye'. The strong airflow leaving the ice edge has high stability (see the bright area to the lower left left of the 'eye'), but quickly de-stabilised downwind due to the strong sensible heat flux from the relatively warm ocean.

According to numerical models for polar low development [*Nordeng & Rasmussen* 1992; *Okland* 1989; *Heinemann & Claud* 1997], both the region of low level shallow convection confined by a capping inversion and the region of deep convection, may be important for the development of polar MCs. Figure 1 shows that Radarsat images may be used to distinguish the fine structure of the wind field over different stability and convective regimes. This capability, combined with existing satellite and numerical studies of polar MCs [*Heinemann & Claud* 1997], may be useful for studying the driving mechanisms for initiation, development, and maintenance of polar MCs. The retrieval of the low-level wind field structure from Radarsat images of polar MCs may help to improve the numerical simulation and forecasting of MCs. A difficulty in quantifying the intensity of oceanic deep convection is to know both the intensity and area of sea to air heat and moisture transfers that are driving the convection by cooling the surface waters. The surface structures in the wind field (the fluxes are proportional to the strength of the wind and the air-sea temperature difference) seen by the SAR can be interpreted with simple boundary layer models to provide quantitative estimates of the fluxes over extended periods of time.

Figure 2 shows a case from 15 January 1998 in the Labrador Sea close to the Newfoundland coast. The sea-level pressure charts for this date show a

Ascending pass Radarsat ScanSAR wide image of Labrador Sea showing the island of Newfoundland and the Labrador coast acquired 15 Jan.1998 at 21:18 UTC. The image covers 500 · 1450 km and was supplied courtesy of Canadian Ice Services. (SAR data ©CSA 1998).

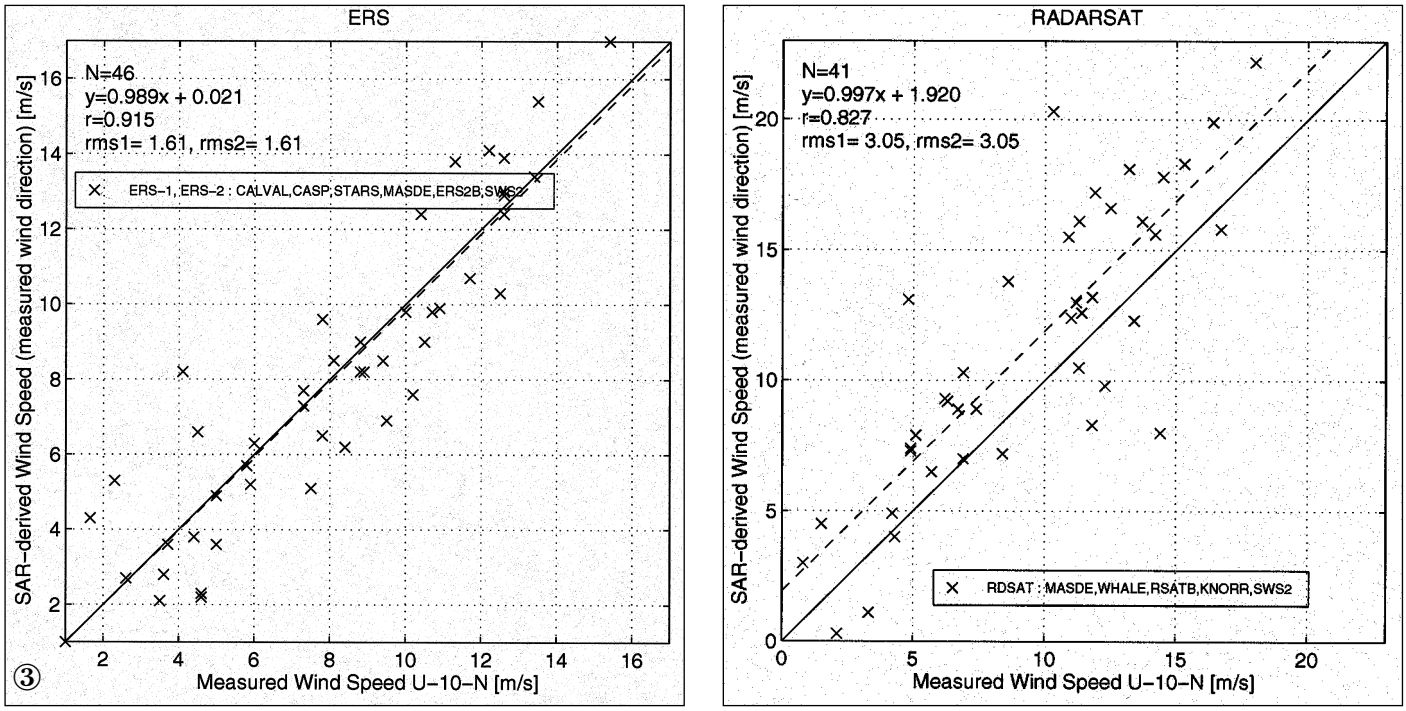

Wind retrieval validation results comparing SAR-retrieved wind S-s with collocated measurements by ships and buoys for (a) the ERS SARs and (b) the Radarsat SAR (right). The wind direction used in the retrieval was from the in-situ measurement. The dashed line is the best-fit line; r is the correlation coefficient; rms1 is the root-mean-squared difference between the two wind speed measurements; rms2 is the root-mean-squared error in the SAR retrieval with respect to the best-fit line.

closed synoptic low centred north of Newfoundland. As in the previous case, the regions of deep cellular convection (north of the 'eye') and strong stable flow advected from the land (bright area below the 'eye') are apparent. The strong airflow is separated from the calmer wind (dark area) with a sharp spiral-form frontal boundary converging to the calm and warm 'eye' of the MC. Note that the frontal boundary curves across the landmass and is contiguous offshore further to the north. Lee waves are seen downwind of Newfoundland.

Ships and buoys

Unfortunately, Radarsat ScanSAR images such as those of Figures 1 and 2 are not yet operationally calibrated. This situation will improve, allowing extraction of both the wind field structure and wind speed from this type of image. Over the past 7 years, we have acquired a number of SAR datasets, both ERS and Radarsat, for validation of SAR wind retrieval models [see e.g. *Vachon & Dobson* 1996].

In Figure 3, we present our ERS and Radarsat single-beam wind retrieval results, as available to date. In each case, the SAR image was collocated with the *in-situ* measurement location and was within less than one hour (and generally, less than 15 minutes) of the validation measurements. The SAR images were processed on a workstation-based SAR processor at CCRS. The processor accounts for analog-to-digital converter power loss by carrying out a saturation analysis of the raw signal data and applying gain corrections prior to range and azimuth compression. This correction is particularly important for the ERS-1 SAR. The processor was calibrated using images of calibration transponders acquired over several years of use. The SAR wind speed was retrieved using the radar cross-section at the buoy location and a scatterometer wind retrieval model. For the C-band VV polarisation ERS SARS, we used CMOD IFR2 [*Ifremer-Cersat*, 1996]. This model was developed for off-line processing of the ERS Scatterometers and is based on comparison of the 50-km resolution cells with *in-situ* buoy measurements of wind speed. For the C-band HII polarisation Radarsat SAR, we used CMOD IFR2 and converted its cross sections to hybrid HH values using airborne scatterometer polarisation ratios acquired at C-band [*Unal et al.* 1991].

The ERS scatterplot is included here as a baseline for what could be expected from Radarsat. The buoy winds have been corrected to the equivalent neutral stability wind speed at 10-m height above the surface. Across our set of 46 ERS observations covering calm to 15 m/s wind speeds, we found a root-mean-squared (rms) difference between the SAR and *in-situ* wind speeds of 1.6 m/s, when the *in-situ* wind direction is used. This affirms the use of SAR as an imaging scatterometer. The Radarsat result is somewhat poorer. Across our set of 41 Radarsat observations covering calm to 18 m/s wind speeds, we found an rms difference between the SAR and *in-situ* wind speeds of

3 m/s, when the *in-situ* wind direction is used. The retrieved Radarsat wind speeds appear to be biased high, suggesting that the C-band polarisation ratios we have used in our hybrid HH polarisation model are too large.

Conclusion

In this paper, we have presented Radarsat SAR images of mesoscale cyclones and validation results of wind retrieval from both ERS and Radarsat SAR images. These results illustrate the potential role of SAR in understanding and monitoring mesoscale atmospheric and associated oceanic phenomena, such as polar lows and oceanic deep convection. Our wind speed validation results are significantly better for the ERS SARs than for the Radarsat SAR, indicating that our hybrid C-band HH polarisation model for Radarsat SAR wind retrieval requires improvement. For the ERS SARs, we found an rms difference between the SAR wind and the *in-situ* buoy wind of 1.6 m/s.

Acknowledgements

We thank the many individuals and organisations that have contributed to the acquisition and processing of the data that appears in Figure 3. David Bradley and Bruce Rasay (CIS) supplied the Radarsat SAR images of Figures 1 and 2. John Woffe (CCRS) helped with the data processing.

References

Bradley D, B Ramsay, M Manore & M Shokr: Canadian Ice Service Radarsat image archive, to appear in *Proc. 20th Canad. Symp. on Remote Sensing*, 10-13 May 1998, Calgary, Canada.

Businger S & R Reed: Polar Lows. In 'Polar and Arctic Lows', Edited by P Twitchell, E Rasmussen & K Davidson, A DEEPAK Publishing, Hampton, Virginia, USA, pp. 3-47, 1989.

Fetterer F, D Gineris & CC Wackernan: Validating a scatterometer wind algorithm for ERS1 SAR*, IEEE Trans. Geosc. Rem. Sens.* **36**, 479-492, 1998.

Hartmann J, C Kottmeier & S. Raasch: Roll Vortices and Boundary-layer Development during a cold air outbreak. *Boundary-Layer Meteorol*. **84**, 45-65, 1997.

Heinemann 0 & C. Claud: Report of a Workshop on 'Theoretical and Observational Studies of Polar Lows' of the European Geophysical Society Polar Lows Working Group. *Bull. Amer. Meteor. Soc.* **78**, 2643-2658, 1997.

Ifremer-Cersat: Offline wind scatterometer ERS Products: User Manual. Technical Report C2-MUT-W-0l-IF, Version 2.0, Ifremer-Cersat, Plouzane, France, 1996.

Marshall J, F Dobson, K Moore, R Rhines, M Visbeck, E D'Asaro, K Bumke, S Chang, RA Clarke, R Davis, K Fischer, R Garwood, P Guest, C Herbaut, T Holt, J Lazier, S Legg, R Pickart, M Prater, I Renfrew, F Schott, U Send & R Smethie: The Labrador Sea Experiment. In press, *Bull. Amer. Meteorol. Soc.*, 1998.

Mitnik L, M Hsu & M Mitnik: Sharp gradients and organized structures in sea surface wind field in the regions of polar vortex formation. *The Global Atmos. & Ocean Sys.* **4**, 335-361, 1996.

Nordeng T & E Rasmussen: A most beautiful low. A case study of a polar low development in the Bear Island region. *Tellus* **44A**, 81-99, 1992.

Okland H: On the Genesis of Polar Lows. In 'Polar and Arctic Lows', Edited by P Twitchell, E Rasmussen & K Davidson, A DEEPAK Publishing, Hampton, Virginia, USA, 179-191, 1989.

Twitchell P, E Rasmussen & K Davidson (editors): Polar and Arctic Lows. A DEEPAK Publishing, Hampton, Virginia, USA, 421 p, 1989.

Unal CM, P Snoeij & PJF Swart: The polarization-dependent relation between radar backscatter from the ocean surface and surface wind vector at frequencies between 1 and 18 GHz. *IEEE Trans. Geoscience Rem. Sens.* **29**, 621-626, 1991.

Vachon PW & FW Dobson: Validation of wind vector retrieval from ERS-1 SAR images over the ocean. *The Global Atmos. & Ocean Sys.* **5**, 177-187, 1996.

Wackerman C, C Rufenach, R Shuchman, J Johannessen & K Davidson: Wind vector retrieval using ERS-1 Synthetic Aperture Radar imagery. *IEEE Trans. Geosc. Rem. Sens.* **34**, 1343-1352, 1996.